

Characteristic Features of Vector Chaos

R. Delbourgo and R. B. Zhang

Department of Physics, University of Tasmania,
G.P.O. Box 252C, Hobart, Tas. 7001, Australia.

Abstract

Quadratic maps of a vector, depending on a *vector* parameter and any number of scalars, can be reduced to the transformation $x \rightarrow ax(1-x) + dy^2$ and $y \rightarrow h(c-x)y$, where $d = 0, 1$ or -1 . Such a (3-parameter) set of transformations possesses an extremely rich structure. We have determined the Julia and Mandelbrot sets of this system and have delineated the characteristic types of x - y motion as well as the transition from one regime to the next.

1. Introduction

One-dimensional unimodal maps as well as circle maps have been exhaustively studied and an enormous body of knowledge about their properties has accumulated (Collet and Eckmann 1980; Iooss *et al.* 1983; Hao 1984; Cvitanovic 1984; Holden 1986). Two-dimensional maps have also received considerable attention and none more so that the Henon (1976) map, which produced one of the first examples of a strange attractor. Helleman (1980) has studied many such two-component maps and has managed to reduce almost all cases to his 'standard' quadratic form:

$$x' = 2x(C+x) + y, \quad y' = -Bx, \quad (1)$$

which certainly encompasses the one-dimensional logistic map and the Henon map, in another guise. He has studied (1) in considerable detail and described the period-doubling and strange regimes of the system.

In this paper we shall start *ab initio* with a bonafide *vector* variable \mathbf{r} and discuss the nonlinear maps which it can undergo, which specifically depend on an external *vector parameter* and any number of scalars. Then we concentrate on the quadratic maps and show that they can be reduced to the canonical form

$$x \rightarrow ax(1-x) + dy^2, \quad y \rightarrow b(c-x)y, \quad (2)$$

where d either vanishes or can (by scaling y) take the values ± 1 . Such maps can produce many different types of \mathbf{r} behaviour and this can be discerned from their Julia and Mandelbrot sets, which we examine next. In fact the situation leads to such complexity that, in this paper, we shall content ourselves by

describing the various motions of the vector field, depending on the ranges of the (three) parameters in question, and limiting the quantitative study to only the most rudimentary aspects—those that can be exactly calculated without any approximations. We should point out that in general the vector map (2) is *not reducible* to the Helleman form (1) and the only case where it can be made to coincide is for $d = 0$, when the map becomes effectively one-dimensional anyway, and thus uninteresting from our point of view. In a future paper we shall treat the quantitative features much more fully, and try to derive the universal properties of these vector maps by analogy with what has already been achieved for Hamiltonian systems of two variables.

2. Vector Variables and Parameters

Let \mathbf{r} denote the vector variable. If one assumes that it depends purely on scalar parameters, collectively denoted by λ , then the only conceivable, rotationally covariant map can be written as

$$\mathbf{r}' = \mathbf{r}A(r^2, \lambda),$$

where A is a scalar function of its arguments. Because the direction of \mathbf{r} is unchanged, the map is essentially one-dimensional and solely affects the length r . In particular, if we have just one scalar parameter λ or the map is quadratic, it can be reduced to the canonical logistic form,

$$r' = \lambda r(1 - r), \quad (3)$$

whether or not \mathbf{r} is an axial or polar vector.† Everything worth knowing about (3) has been discovered by now, so we pass to problems where the external parameters are intrinsically vectorial.

Suppose that there is a single vector influence, labelled \mathbf{n} . Because the length of \mathbf{n} is just another scalar which can be absorbed in the set λ , we shall regard \mathbf{n} as a unit vector in what follows. The most general map can thereby be expressed as

$$\mathbf{r} \rightarrow \mathbf{r}' = \mathbf{r}A + \mathbf{n}B + \mathbf{n} \times \mathbf{r}C, \quad (4)$$

where A , B and C are scalar functions of r^2 and $\mathbf{r} \cdot \mathbf{n}$, plus of course all the scalars λ . For simplicity, let us assume that the map is parity preserving;‡ then we can distinguish between two cases:

- (i) \mathbf{r} and \mathbf{n} are both polar or axial vectors. Hence C must disappear altogether from (4).
- (ii) \mathbf{r} and \mathbf{n} have opposite parity, one being axial and the other polar. Here A and C must be even functions while B must be an odd function of $\mathbf{n} \cdot \mathbf{r}$.

† Recall that under space reflection, or a 'parity transformation', a polar vector-like momentum changes sign but an axial vector such as torque does not. This distinction is made when we consider cases (i), (ii) and (iii) below.

‡ That is to say, \mathbf{r} and its mapped \mathbf{r}' , transform in the *same way* under space inversion. The dynamics are 'parity-preserving'.

Further progress is impossible, until we spell out the nature of the map or tie it to some physical example.

Let us therefore focus on functions that are at most quadratic in \mathbf{r} . Case (ii) then reduces to

$$\mathbf{r} \rightarrow \mathbf{r}' = a\mathbf{r} + b\mathbf{n}(\mathbf{r} \cdot \mathbf{n}) + c\mathbf{n} \times \mathbf{r}$$

and, since it is linear, is undemanding. Case (i) offers much brighter prospects, however, insofar as it is a proper quadratic map and allows us to introduce at most six scalar constants (labelled by a, b, c, e, f, g):

$$\mathbf{r} \rightarrow \mathbf{r}b(c - \mathbf{n} \cdot \mathbf{r}) + \mathbf{n}\{a\mathbf{r}^2 + g + e(\mathbf{n} \cdot \mathbf{r})^2 + f(\mathbf{n} \cdot \mathbf{r})\}.$$

We use the freedom in translating the origin by shifting it along \mathbf{n} and thereby eliminating the constant g . Then, we rescale the component of \mathbf{r} along \mathbf{n} so that $e + b + d + f = 0$. Lastly, we use the identity $r^2 = (\mathbf{r} \cdot \mathbf{n})^2 + (\mathbf{r} \times \mathbf{n})^2$ to express the map in the canonical form

$$\begin{aligned} \mathbf{r} \rightarrow \mathbf{r}b(c - \mathbf{n} \cdot \mathbf{r}) + \mathbf{n}\{a\mathbf{n} \cdot \mathbf{r}(1 - \mathbf{n} \cdot \mathbf{r}) + b(1 - c)\mathbf{n} \cdot \mathbf{r} + d(\mathbf{n} \times \mathbf{r})^2\} \\ = \mathbf{n}\{a\mathbf{n} \cdot \mathbf{r}(1 - \mathbf{n} \cdot \mathbf{r}) + d(\mathbf{n} \times \mathbf{r})^2\} + b(\mathbf{n} \cdot \mathbf{r} - c)\mathbf{n} \times (\mathbf{n} \times \mathbf{r}), \end{aligned} \quad (5)$$

which now contains just *four* constants. Since one can always direct \mathbf{n} along the x -axis, the map reduces to the advertised form as far as the x and y components are concerned. Furthermore, since the second equation is homogeneous in y , we can always rescale the first one so that $d = \pm 1$, unless it happens that $d = 0$ at the beginning. This then establishes that vector quadratic maps can always be expressed in the form (2) with $d = 0$ or ± 1 .

Before leaving this section we ought to point out that higher order, nontrivial, polynomial maps do exist for case (ii) and deserve a study in their own right. However, these are *exceedingly complicated*; even at cubic level one has to contend with some six independent control constants, even after rescaling and shifting origin. Clearly the simplest case, namely (2), needs to be explored first,† if for no other reason than to find out what features must be followed up in more intricate vector problems.

3. Fixed Points of the Vector Map

If the map begins with \mathbf{r} directed along \mathbf{n} so that y is rigorously zero, the system stays one-dimensional and has all the features of the logistic map. The same thing happens if b is zero or sufficiently small that y tends to the fixed point $y^* = 0$; this will occur if we have for the n -cycle product

$$\left| \prod_{i=1}^n b(c - x_i^*) \right| < 1, \quad (6)$$

† Some physical problems where (5) has relevance are:

- (i) the velocity of a charged particle in a plasma under the influence of a periodic electric field;
- (ii) the vorticity of a point in a magnetohydrodynamic medium due to an oscillating magnetic field;
- (iii) the angular momentum of a system due to a periodically applied torque, etc.

In each of these cases the vector influence (\mathbf{n}) and the measured vector quantity (\mathbf{r}) have the same parity.

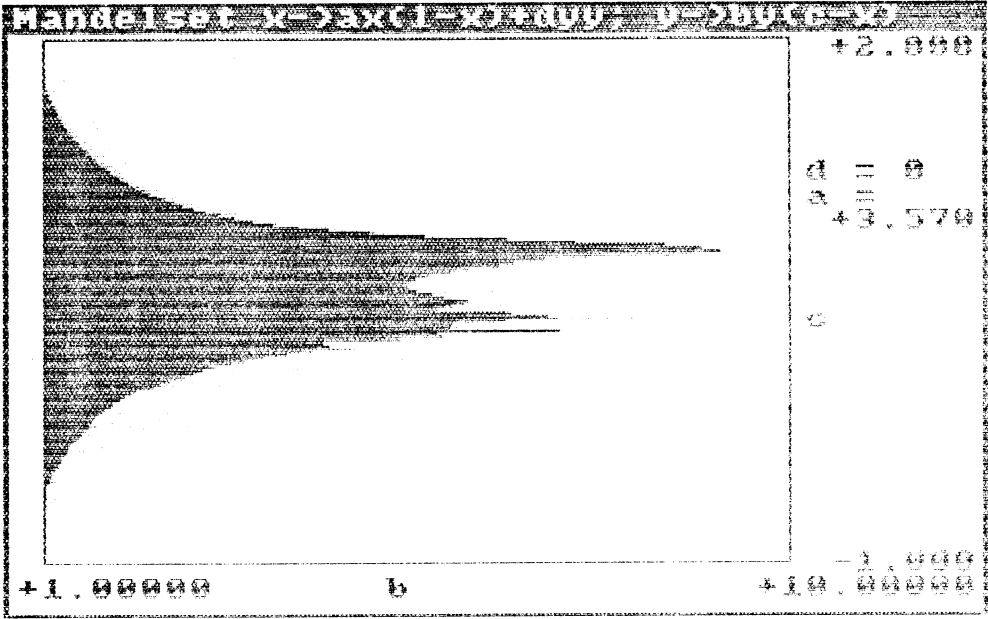


Fig. 1. Mandelbrot set in b and c for the vector map, with a held fixed at 3.57 and $d=0$.

where the fixed x^* values are purely governed by the value of a . A related case arises when $d=0$; in that circumstance x decouples totally from y and x^* runs between 0 and 1 . The fixed points in y depend on the seed y value and on the a value (which fixes the x behaviour). In particular, one can easily appreciate that an m cycle in x can lead to (i) a divergence in y (because b is large enough), (ii) an m cycle in $|y|$ if b is at the boundary of (6), or (iii) a single fixed point at $y^*=0$ if (6) is obeyed. If x behaves erratically, then so will y , providing one is at the edge of (6) as $m \rightarrow \infty$, and the only way to ascertain this is to examine the Mandelbrot set; a typical one is shown in Fig. 1 where b and c are varied and a is set equal to the chaotic two-cycle limit value, $a=3.57$. Here, as in other cases, a parameter region of convergence for r is clearly discernible. The Julia set in Fig. 2a merely confirms that y will fluctuate with x but remain finite even in this chaotic x regime.

The Julia sets shown in Figs 2b and 2c indicate the drastic effect of taking d different from zero; $d=-1$ especially enlarges the domain of convergence. Assuming now that $d \neq 0$, it is rather trivial to work out the constraints on the parameters which guarantee that there is a *unique attractor* r^* . In that event we have

$$x^* = c - 1/b \quad \text{and} \quad y^{*2} = x^*(1 - a + ax^*)/d, \tag{7}$$

providing y^* is not zero; as well we must ensure that the magnitudes of the two eigenvalues of the first mapping derivative matrix

$$\frac{\partial r'}{\partial r} = \begin{pmatrix} a(1 - 2x^*) & 2dy^* \\ -by^* & b(c - x^*) \end{pmatrix} \tag{8}$$

do not exceed 1. It is straightforward to show that this leads to

$$-1 - bdy^{*2} \leq a(1 - 2x^*) \leq 1 - 2bdy^{*2}, \quad (9)$$

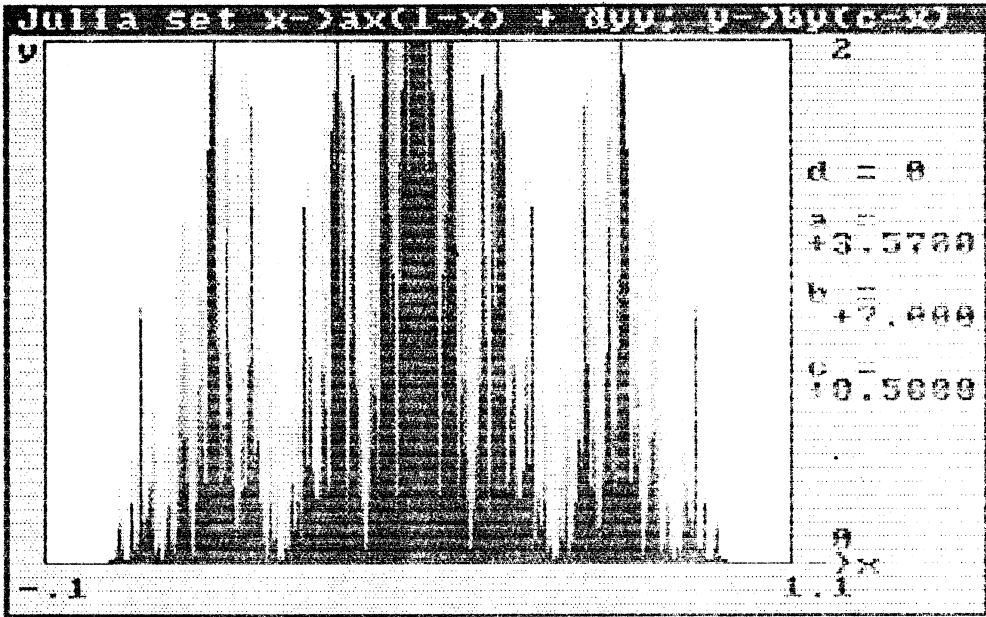
with $bdy^{*2} \leq 2$. The lower bound in (9) amounts to the condition that at least one of the eigenvalues has reached -1 , while at the upper bound both eigenvalues are complex with modulus unity, and thus $\det(\partial \mathbf{r}' / \partial \mathbf{r}) = 1$; as an illustration of these conditions, see Fig. 3. The fixed parameters are taken to be $b = 3.6$, $c = 1$ and $d = 1$, and a is varied in small steps from about 2 to 4. The unique attractor, given by (7), lies at $x^* = 0.7222$, providing that a runs between the lower limit of 2.2235 and the upper limit of 3.0857, according to (9), whereupon y^* runs from 0.5255 to 0.321. This is confirmed in Fig. 3, but much more striking and interesting is the motion of \mathbf{r} *outside* this range; noticeable are (distorted) elliptic trajectories below $a = 2.2235$ and period-doubling bifurcations above $a = 3.0857$. This behaviour is readily understood analytically; the lower a values correspond to complex eigenvalues of (8), while the upper a values are associated with one eigenvalue greater than one and the other less than one—hence the shrinkage to one effective degree of freedom and the one-dimensional bifurcation scenario. We now explain in more detail how this transpires and what happens in more extreme ranges of the parameters.

4. Vector Bifurcations

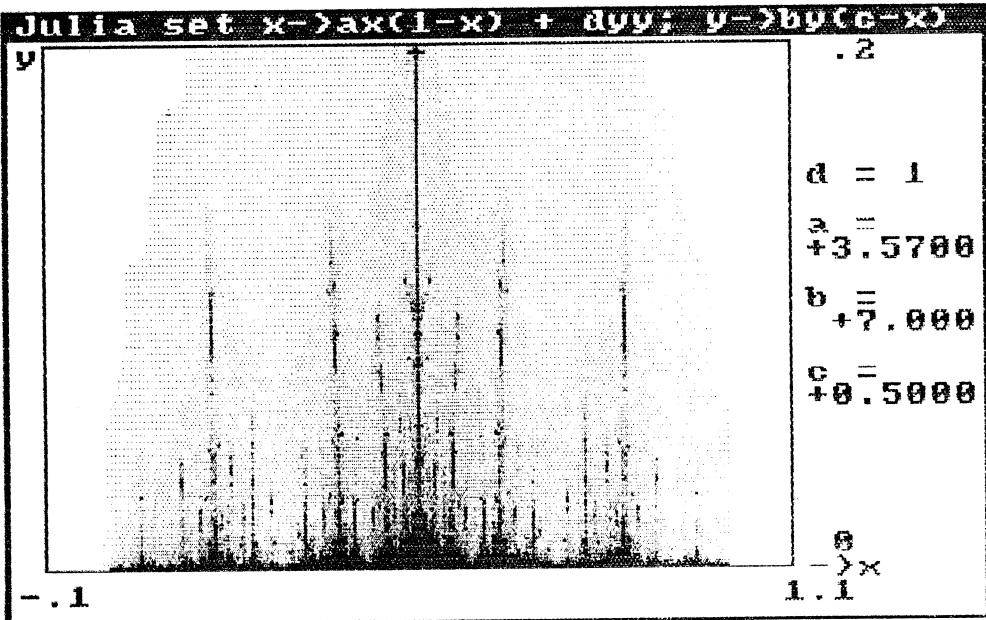
Because we are free to vary the three parameters of our problem when investigating the various regimes of vector behaviour, it is easy to get lost in the multiplicity of features that emerge. It makes good sense at first to set $d = 1$, fix two of the parameters, and consider the remaining parameter as the single control variable. Later on, after we have classified the regimes, we see that similar behaviour arises when some or all of the parameters are changed in a regular manner. Altering the sign of d does not substantially change the classification, since the operative variable is really the product bd .

For the moment let us follow the changing nature of the map with a , holding b , c and $d (=1)$ fixed. By examining the eigenvalue λ equation for the matrix derivative (8), we find that $|\lambda| < 1$ provided that (9) is obeyed and the one fixed point \mathbf{r}^* is determined by (7). Now let us overstep the ranges in (9). If $a(1 - 2x^*)$ is marginally less than $-1 - bdy^{*2}$, one (real) eigenvalue drops below -1 , while the other's magnitude remains less than 1. This means the disappearance of one mode, with the other mode going through the traditional period-doubling cascade—as precisely happens in Fig. 3 when a exceeds the critical value 3.0857, given the chosen b and c . The onset of the four-cycle can even be pinpointed although the equations resist easy algebraic solution: this exercise requires us to consider the double map associated with the first bifurcation,

$$\begin{pmatrix} x_{\mp} \\ y_{\mp} \end{pmatrix} = \begin{pmatrix} a(1 - x_{\mp}) & dy_{\pm} \\ -by_{\pm} & bc \end{pmatrix} \begin{pmatrix} x_{\pm} \\ y_{\pm} \end{pmatrix},$$

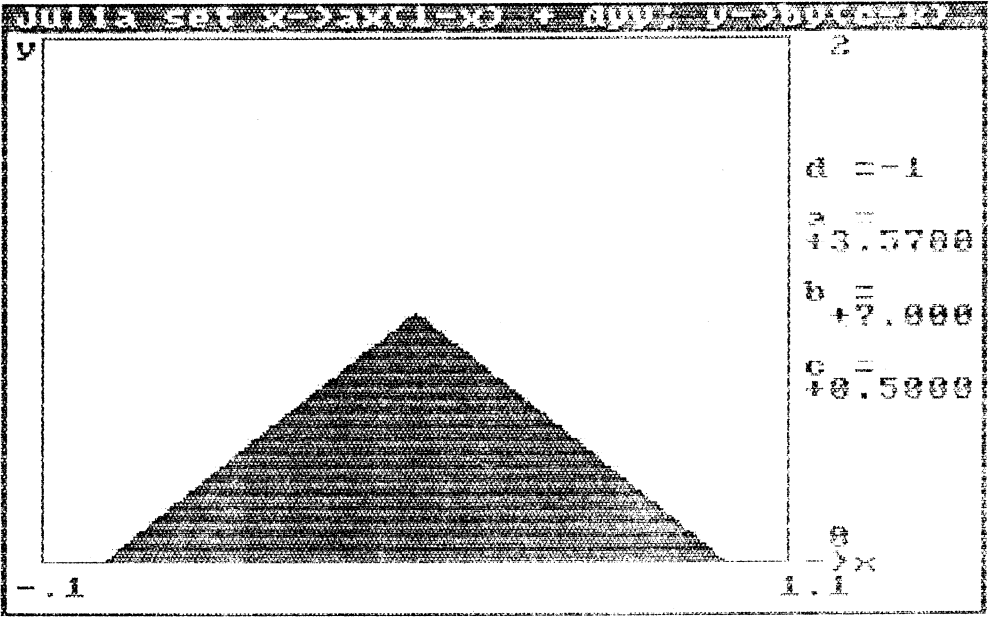


(a)



(b)

Fig. 2. Julia set in r with the parameters fixed at $a = 3.57$, $b = 7$ and $c = 0.5$; (a) $d = 0$; (b) $d = 1$; and (c) $d = -1$. In (b) and (c) note the reduction and enlargement respectively of the convergence domain relative to (a).



(c)

Fig. 2 (Continued)

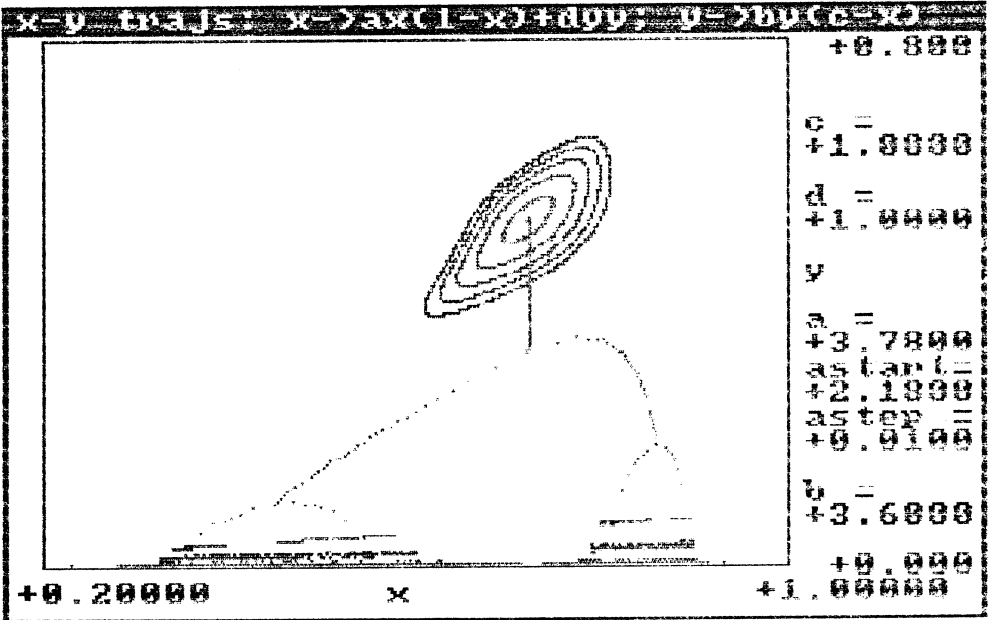


Fig. 3. Fixed points of r as a is varied in steps of 0.01 from 2.18 to 3.78; $b=3.6$, $c=1$ and $d=1$. Note the flip bifurcations at the bottom and the Hopf bifurcations at the top.

and factor out the (unstable) fixed points at $r = 0$ and r^* found before. After a little work, the remaining equation can be reduced to a quadratic, yielding the roots

$$x_+ = c - \zeta/b, \quad x_- = c - 1/\zeta b, \quad dy_{\pm}^2 = x_{\mp} - ax_{\mp}(1 - x_{\mp}), \tag{10}$$

where ζ is determined in terms of the parameters by

$$\zeta = b\omega + (b^2\omega^2/4 - 1)^{\frac{1}{2}} \quad \text{and} \quad \omega = c - \frac{1}{2} + (\frac{1}{4} + 1/b^2 - c/a)^{\frac{1}{2}}.$$

The four-cycle develops when one eigenvalue of the first derivative of the double map attains -1 , namely when the lower eigenvalue of

$$\begin{pmatrix} a(1 - 2x_+) & 2dy_+ \\ -by_+ & b(c - x_+) \end{pmatrix} \begin{pmatrix} a(1 - 2x_-) & 2dy_- \\ -by_- & b(c - x_-) \end{pmatrix}$$

equals -1 . This happens when

$$1 + a^2(1 - 2x_+)(1 - 2x_-) + 2bdy_+y_-(2bdy_+y_- - 1) + ab^2d\{y_+^2(c - x_-)(1 - 2x_-) + y_-^2(c - x_+)(1 - 2x_+)\} = 0. \tag{11}$$

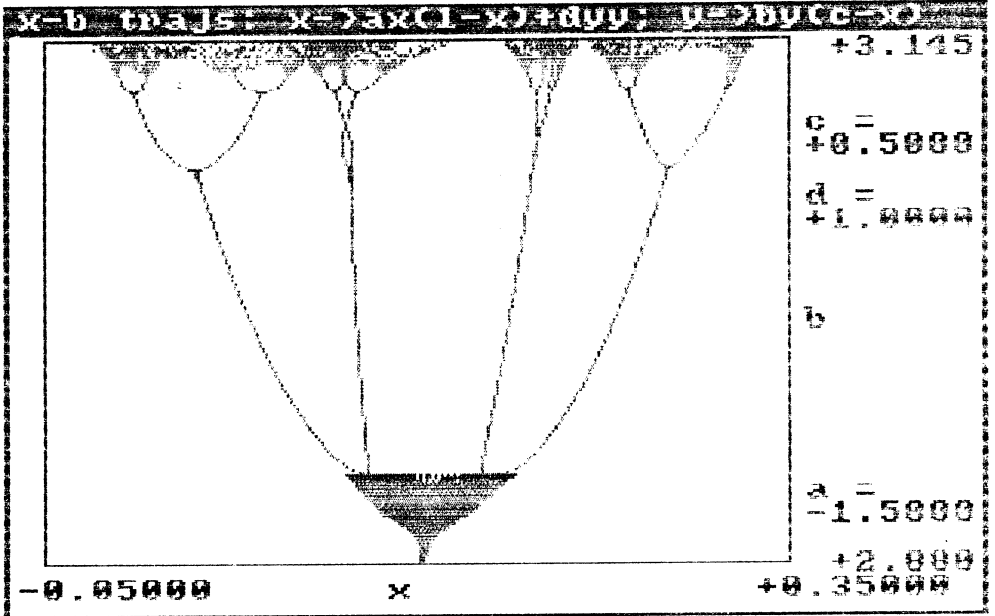
The combination of (10) and (11) provides one condition on a, b, c, d . Thus, given b, c and d , the value of a at which the four-cycle starts can be worked out. We have not been able to solve the equations algebraically (except in the limit $bd = 0$ when the correct value $a = 1 + \sqrt{6}$ does emerge) and have therefore resorted to numerical methods. With the numbers $b = 3 \cdot 6, c = 1$ and $d = 1$ used in Fig. 3 we have derived the four-cycle point as $a = 3 \cdot 4546, x_- = 0 \cdot 4448, x_+ = 0 \cdot 8610, y_- = 0 \cdot 0887, y_+ = 0 \cdot 1773$; these values agree perfectly with the computer graphics and give us confidence in the analysis. To tackle eight cycles and more requires superhuman effort, so the computations are best left to the machine.

At the other end of the fixed line, when $a(1 - 2x^*)$ is marginally greater than $1 - 2bdy^{*2}$, the fixed point changes into a *fixed path* which starts off elliptical (it is basically the Hopf circle) and suffers progressive distortion as a moves down—indeed at certain values of a , such as $2 \cdot 1006$, the attractive orbit looks strange. This Hopf bifurcation is readily comprehended. Because the elliptic scales as governed by the square root of

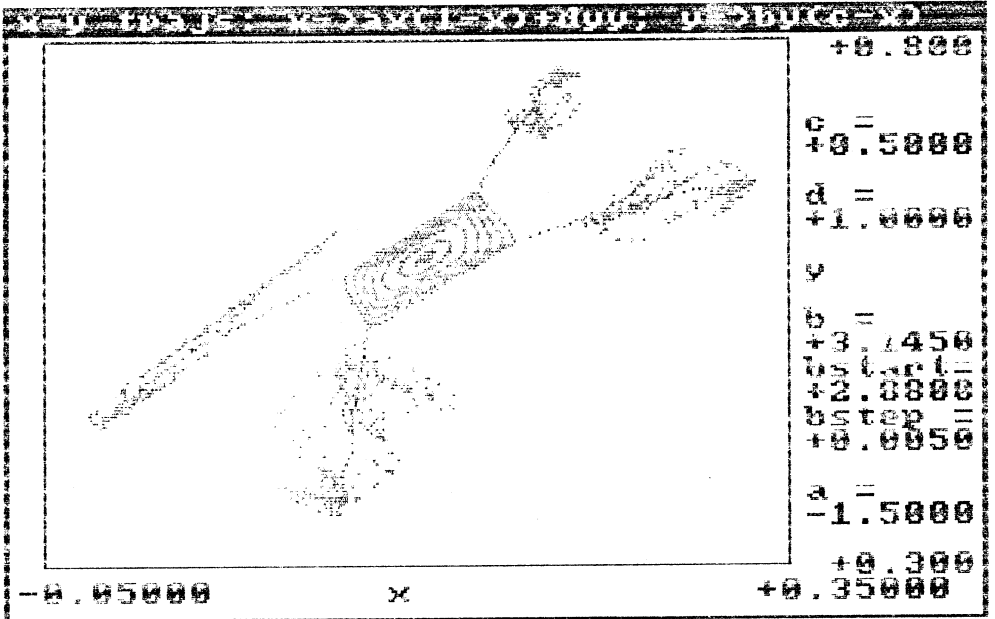
$$\Delta a = a - (1 - 2bdy^{*2}) = a - a_c, \tag{12}$$

just like the first flip bifurcation in one-dimensional maps, let

$$x = x^* + \xi(-\Delta a)^{\frac{1}{2}} + O(\Delta a), \quad y = y^* + \eta(-\Delta a)^{\frac{1}{2}} + O(\Delta a), \tag{13}$$



(a)



(b)

Fig. 4. (a) x -projection of a four-cycle and subsequent flip bifurcations as b is varied near 3; $a = -1.5$, $c = 0.5$ and $d = 1$ here. (b) Full \mathbf{r} trajectories showing how the four-cycle emerges from the orbits as b is varied. The ellipses develop into a 'rectangle' which buds off into the four-cycle when b exceeds the critical value.

and consider the iteration scheme to order $(-\Delta a)^{\frac{1}{2}}$:

$$\begin{pmatrix} \xi' \\ \eta' \end{pmatrix} = \begin{pmatrix} a_c(1-2x_c) & 2dy_c \\ -by_c & 1 \end{pmatrix} \begin{pmatrix} \xi \\ \eta \end{pmatrix}. \tag{14}$$

Here r_c is the single fixed point at the very edge of instability $a = a_c$. One readily finds that the unimodular map (14) has the invariant conic

$$b\xi^2 - 2bdy_c\xi\eta + 2d\eta^2,$$

which accurately describes the eccentricity and inclination of the ellipses that sprout for $a < a_c$; the scale is of course set by $(a_c - a)^{\frac{1}{2}}$. When a is substantially below a_c , the invariant curves become badly distorted and displaced and r is no longer evenly distributed on them; indeed as a is reduced further, the features become quite striking. This forms the subject of the next section.

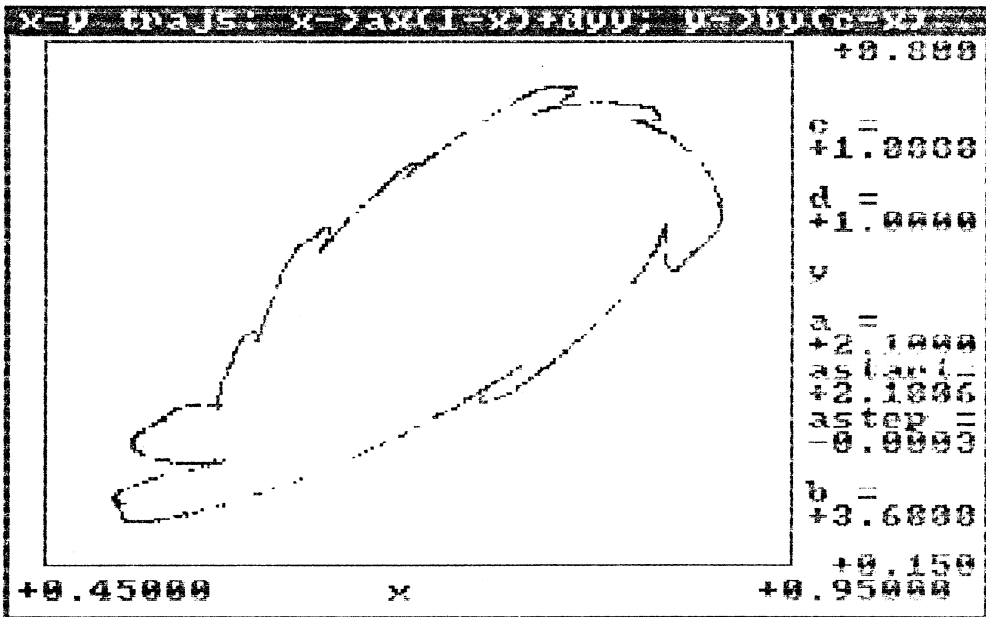
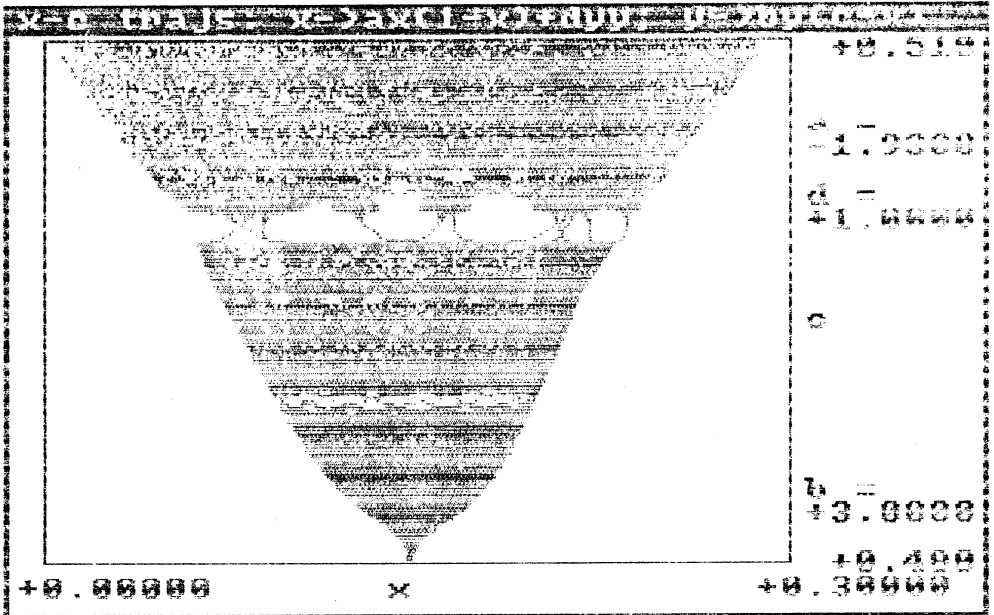


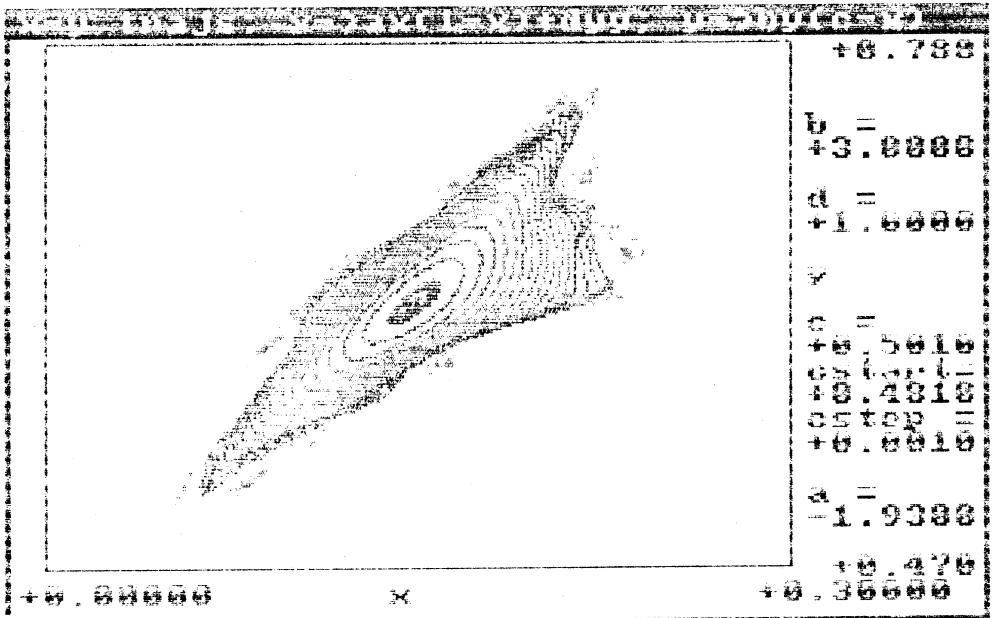
Fig. 5. Formation of cusps as a multicycle is born; a is in the vicinity of 2.1 and $b = 3.6$, $c = 1$ and $d = 1$.

5. Multicycles, Islands and Strange Attractors

By restricting the parameters appropriately, what we have found so far is that the vector r tends to a fixed point r^* , or to a fixed open line after flip bifurcation, or to a fixed closed line after Hopf bifurcation. Sometimes r can tend to fixed points along these lines when the parameters equal special values; this phenomenon is well understood for one-dimensional maps

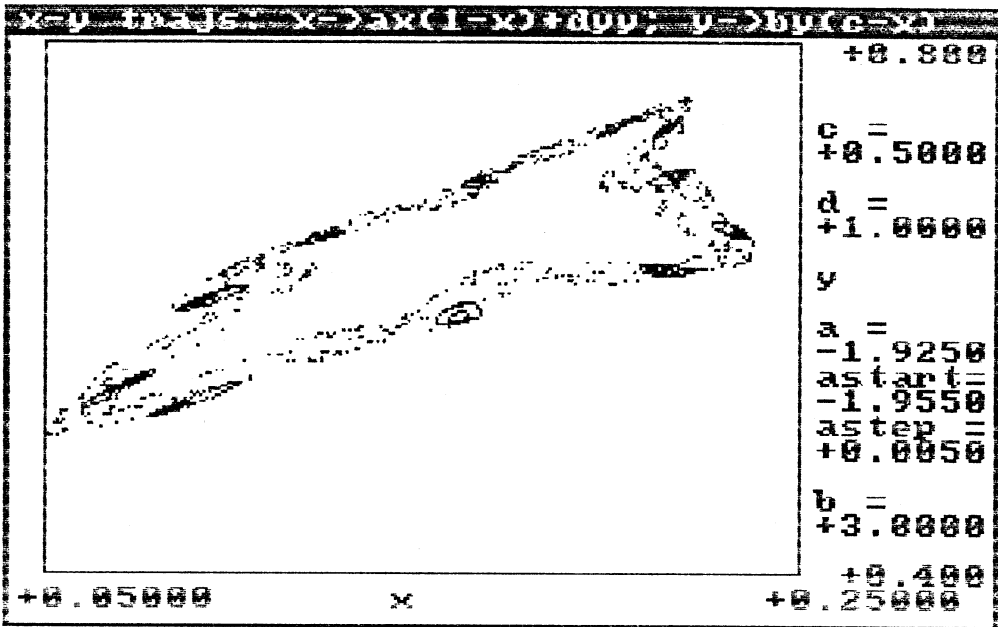


(a)

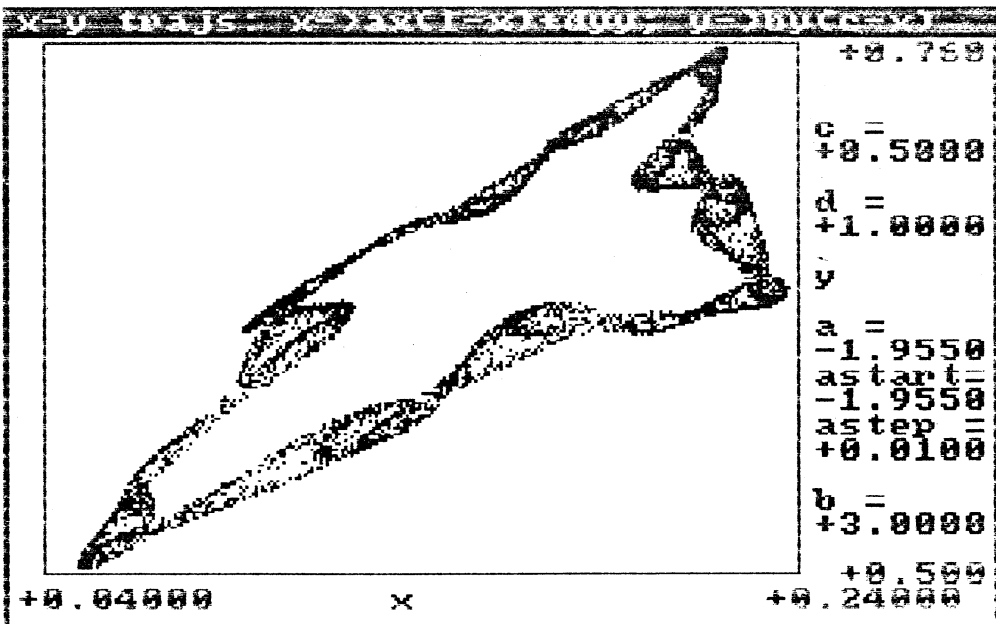


(b)

Fig. 6. (a) Fixed points of x as c is varied with the other parameters held at $a = -1.93$, $b = 3$ and $d = 1$. Note the 11-cycle window near the middle and the way they bubble out—a sign that they are Hopf bifurcating. (b) The r trajectories near the 11-cycle region of Fig. 6a. Observe how the 11 fixed points clearly change into 11 islands as c increases.



(a)



(b)

Fig. 7. Emergence of the 11 islands, seen from the point of view of a variation in a , with the other parameters kept constant. (b) Development of the 11 islands into a strange(?) attractor as a reaches -1.955 ; with $b=3$, $c=0.5$ and $d=1$.

associated with the open line and, with the closed orbit, it corresponds to the behaviour seen in circle maps because the effective degree of freedom is necessarily an angle. In the latter case the way the fixed cycle develops can be arresting. For instance in Fig. 4a we have plotted the spread in the coordinate $x = r \cdot n$ as b is varied near 3 for $a = -1.5$, $c = 0.5$ and $d = +1$; the appearance is not particularly astonishing. However, if we view the same region from a two-dimensional perspective and plot the full x - y trajectories, as in Fig. 4b, the picture is more dramatic. One finds that just before the onset of the four-cycle the orbit develops corners and r spends most of its time in those corners, displaying 'intermittency', until the cycle buds off as parameter b is increased further (it then goes on to flip bifurcate etc. in this particular example). Lauwerier (1986) has discovered similar phenomena in his predator-prey and delayed logistic map models.

This sort of behaviour is quite frequent: just before the onset of a cycle the orbit tends to develop cusps. Fig. 5 is a further illustration of the phenomenon; there we hold fixed $b = 3.6$, $c = 1$ and $d = 1$, and vary a near 2.1 where a 22 cycle is lurking. The same kind of thing can happen when another parameter is varied. In Figs 6a and 6b we depict the emergence of an 11 cycle as c is varied near 0.5 when $a = -1.93$, $b = 3$ and $d = 1$. What is more, we notice the development of the 11 fixed points into 11 'islands' as c is gradually increased.

The subsequent breakup of a multicycle is sensitively dependent on the parameter values; for example in Fig. 4 we observed flip bifurcation, while

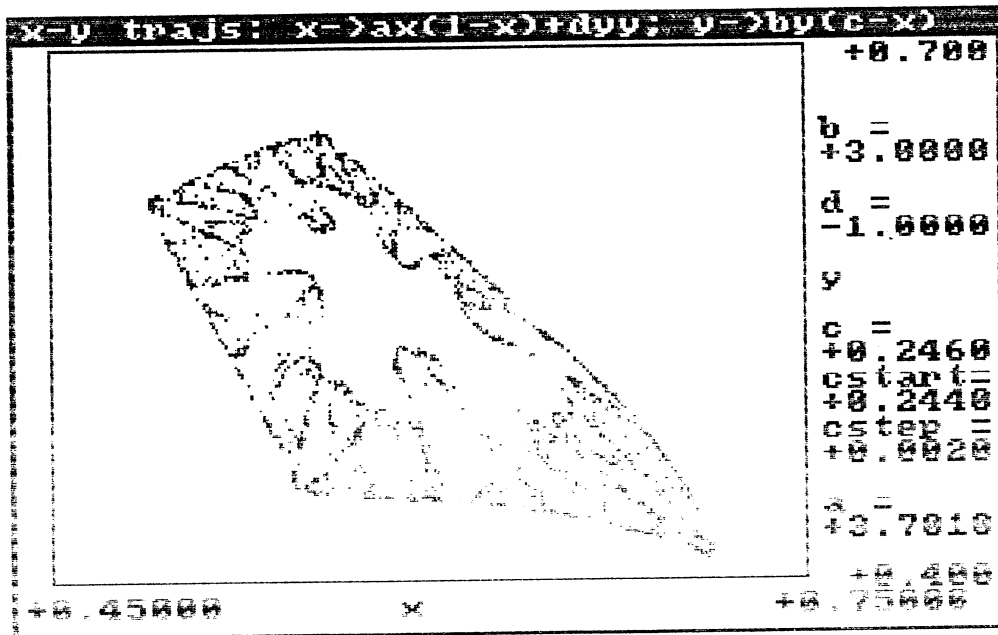
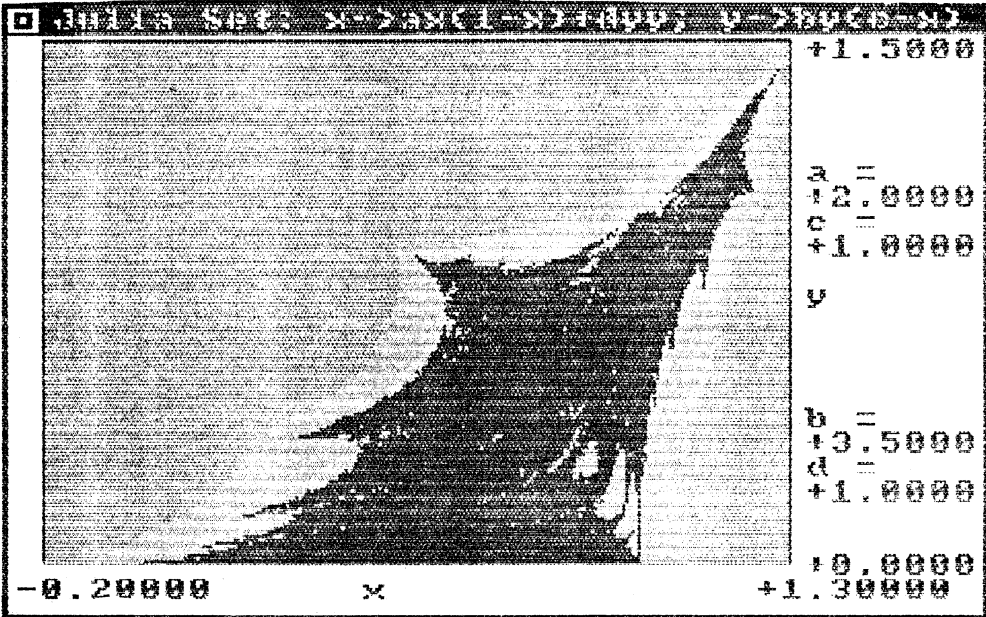
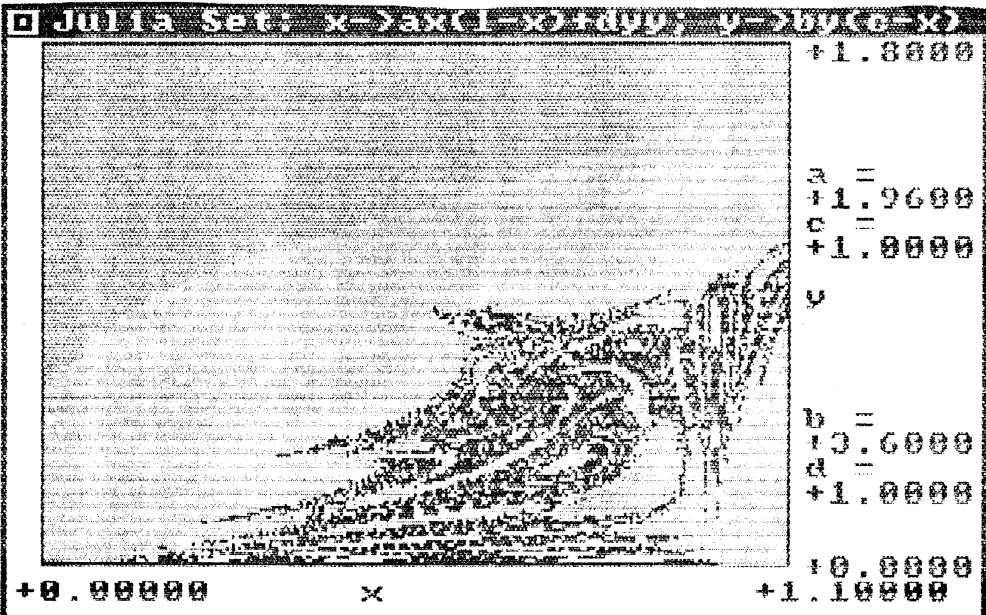


Fig. 8. Another strange looking attractor, this time for $d = -1$; the other parameters are $a = 3.701$, $b = 3$ and $c \approx 0.25$.

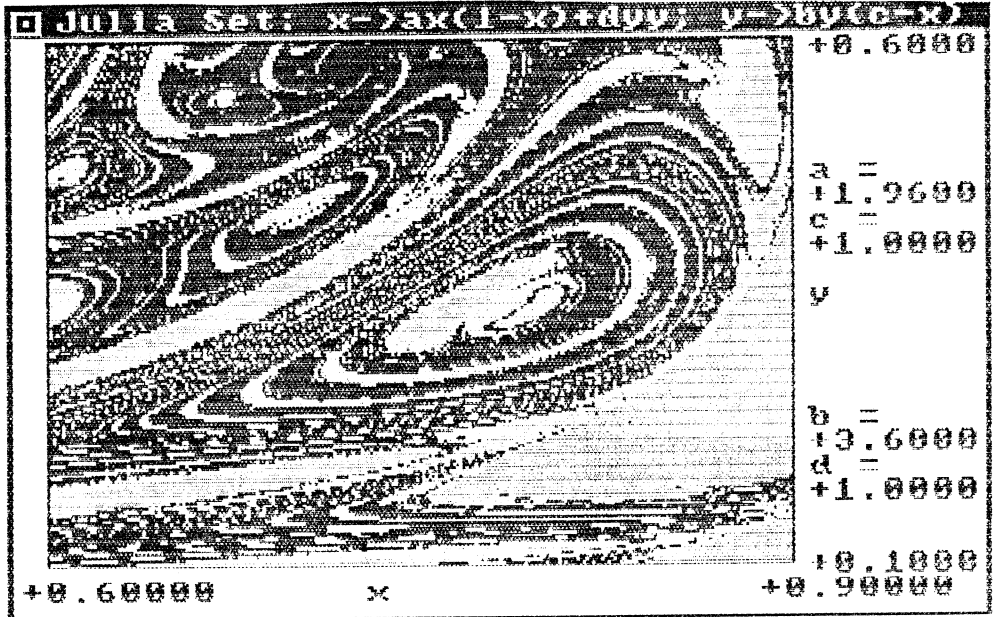


(a)



(b)

Fig. 9. (a) Julia set in r for $a=2$, $b=3.5$, $c=1$ and $d=1$ shows some structure, particularly near the boundary. (b) Julia set in r showing signs of disintegration when a is reduced to 1.96. (c) Enlargement of a portion of Fig. 9b to bring out the fine structure.



(c)

Fig. 9 (Continued)

in Fig. 6 we noticed Hopf bifurcation. (In practical terms, these features are more easily spotted by tracking the spread in a vector component rather than by looking at the full \mathbf{r} trajectory.) What happens after the breakup of the island lines or loops is also sensitive to the parameter ranges. For instance, Fig. 7a depicts an 11 cycle near $a = -1.94$, $b = 3$, $c = 0.5$ and $d = 1$, while Fig. 7b shows how it degenerates into a strange-looking attractor when a reaches the value -1.955 . We have observed similar developments in other instances; Fig. 8 is a case in point and it corresponds to a negative d value, for the first time in this discussion. Such convoluted features arise in the Henon map as well, of course.

Needless to say, situations occur where the parameters lead, as far as we can tell, to a random spread of \mathbf{r} and this will depend delicately on the values of a, b, c, d . To underline this point, we have drawn Julia sets in Fig. 9 showing how a convergence region is sensitively dependent on the seed values of \mathbf{r} , a fact that has considerable practical import when one is searching for attracting regions generally. The intricacies in the resulting plots and the fine structure we have detected are very likely indicative of properties that are universal to other vector maps. We hope to track down the nature and characteristic constants of these universal(?) features in subsequent research.

Acknowledgments

This work was supported by a UR grant. The calculations were carried out on a Commodore-Amiga.

References

- Collet, P., and Eckmann, J. P. (1980). 'Iterated Maps on the Interval as Dynamical Systems' (Birkhauser: Boston).
- Cvitanovic, P. (1984). 'Universality in Chaos' (Adam-Hilger: Bristol).
- Hao, B. L. (1984). 'Chaos' (World Scientific: Singapore).
- Helleman, R. H. G. (1980). *Fund. Prob. Stat. Mech.* **5**, 165.
- Henon, M. (1976). *Commun. Math. Phys.* **50**, 69.
- Holden, A. V. (Ed.) (1986). 'Chaos' (Princeton Univ. Press).
- Iooss, G., Helleman, R. H. G., and Stora, R. (1983). 'Chaotic Behaviour of Deterministic Systems' (North Holland: Amsterdam).
- Lauwerier, H. A. (1986). *In* 'Chaos' (Ed. A. V. Holden), p. 58 (Princeton Univ. Press).

Manuscript received 1 July, accepted 25 November 1988